


Article

Statistical Analysis of the Mathematical Model of Entropy Generation of Magnetized Nanofluid

Munawwar Ali Abbas ^{1,*} and Ibrahim Hussain ² ¹ Department of Mathematics, University of Baltistan, Skardu, Gilgit-Baltistan 16100, Pakistan² Department of Business Management and Commerce, University of Baltistan, Skardu, Gilgit-Baltistan 16100, Pakistan; Ibrahim@uobs.edu.pk

* Correspondence: munawer.abbas@uobs.edu.pk; Tel.: +92-3442312630

Received: 27 May 2019; Accepted: 15 June 2019; Published: 21 June 2019



Abstract: This investigation introduces a mathematical model of entropy generation for Magnetohydrodynamic (MHD) peristaltic wave of nanofluid. The governing equations have been created by the supposition of low Reynolds number and long wavelength estimation. The scientific arrangement has been procured with the help of perturbation technique. The concentration profile, temperature profile, pressure distribution and friction forces are shown graphically for some important parameters. Further, the eventual outcomes of connection between the entropy generation and some various parameters have been plotted by means of correlation and regression. It is fundamental to find the affectability of each parameter on entropy generation.

Keywords: regression; correlation; magnetohydrodynamics; nanofluid; entropy generation

1. Introduction

In fluid mechanics, we think about the conduct of particles at each point inside a space under different physical conditions. Numerical models have been utilized for various sorts of fluids, such as Newtonian fluid [1,2] and non-Newtonian fluid [3,4] to depict the physical marvels in fluid mechanics. There are numerous special instances of non-Newtonian fluid (e.g., nanofluids, micropolar fluids) and numerous studies [5–12] have utilized a certain logical technique to illuminate distinctive kinds of fluids by creating models. Nanotechnology is considered to be an ideal innovative answer for tackling the worldwide energy crisis. Indeed, nanofluid is the fluid suspension of nanostructures, which predominates and guarantees the fundamental amplification of heat transfer properties of the fluid. This helps us to encounter the prospective complexities of fluids in various fluid configuration.

The use of heat transfer fluids is one of the technological applications of nanoparticles, and it possesses an enormous capacity to suspend nanoparticles and confront cooling problems in thermal systems. Due to the great demands placed upon heat transfer fluids in terms of decreasing or increasing energy release to systems, a significant research work was undertaken by Choi and Eastman [13,14] in which a mixture of nanoparticles and base fluid were designated as “nanofluid”. They defined a liquid of ultra-fine particles with sizes less than 100 nm. In the field of thermal engineering and heat transfer, nanofluid has always been an engrossing term. Peristalsis has various applications in connection with nanofluid, such as in engineering, bio-sciences and industries. Several theoretical and experimental attempts in this area have been conducted in the past. Specifically, the works of Latham [15] play a very important role in this connection. Similarly, because of its multiple advantages, research findings on peristaltic flow have received wider applications in industries, and numerous attempts have been made in literature to explore this direction of research. Abbas et al. [16] discussed the application of drug delivery systems under the influence of MHD with peristaltic motion. Bhatti et al. [17] examined the combined effects of MHD and partial slip on the peristaltic flow of nanofluid. Similarly, Salleh et al [18]

studied nanofluid under the influence of magnetic fields in a moving vertical thin needle. A few more magnificent researches can be viewed in the available reference [19–42].

Use of second law investigation in heat design provides a likelihood of advancing a given framework or procedure on the premise of vitality quality, which is altogether different from first law examination. Sustainable power source is the type of vitality determined/gathered from different regular procedures and, as the name proposes, renewable energy sources always recharge inside nature. Specifically, entropy generation investigation amid natural convection heat movement in encased cavities (inside characteristic convection) with different setups has been an area of concentrated examination throughout the previous two decades. Entropy generation determines the dimension of irreversible heat in a procedure. Thus, entropy creation can be utilized as a standard for the evaluating the exhibition of building gadgets. Lately, a huge mass of research has been conducted to check the rate of the entropy generation amid normal convection in different design and ecological applications, for the productive utilization of the accessible vitality. At present, entropy generation advancement is the subject of interests in multiple areas, including heat exchange devices, combustion, electric cooling and permeable media. Rashidi et al. [43] explored the entropy of peristaltic flow in nanofluids with magnetic effects. Mohesen Turabi et al. [44] reviewed entropy generation in a thermal engineering system with solid structures. A comparison table between entropy generation and energy efficiency in natural convection has been analyzed by Pratibha and Tanway [45]. Some later works on entropy generation are [46–50].

Keeping in mind the aforementioned discussion, correlation and regression have not been investigated in any of the aforementioned studies. Therefore, the aim of the present study is to investigate the correlation and regression of entropy generation of MHD peristaltic flow of nanofluid with a porous medium. For this purpose, the study applies the situation of a low Reynolds number and a long wavelength using an analytical technique named the homotopy perturbation method (HPM), which is used to solve the simplified partial differential equations. Expression of temperature, concentration pressure and entropy generation have been obtained graphically. Based on the results of the entropy generation, correlation and regression were derived and explained the role of some pertinent parameters on entropy generation. Due to the vast importance of entropy generation in engineering, exchanging heat devices and electric cooling, this kind of investigation can be much beneficial to finding the sensitivity of each parameter on objective function that is considered to be entropy generation in this model.

2. Mathematical Formulation

We present a demonstration of the peristaltic movement with thick, electrically leading and incompressible nanofluid properties through a two-dimensional, non-uniform channel with sinusoidal wave engendering towards down its wall. As shown in Figure 1, a Cartesian coordinate framework is used so that the x axis is considered alongside the middle line, toward the wave propagation, with y axis traversing to it. The B_0 , a uniform, outer attractive field, is forced along the y pivot and the initiated attractive field is thought to be irrelevant. The geometry of the divider surface is characterized as

$$H(\tilde{x}, \tilde{t}) = \check{a} \sin \frac{2\pi}{\lambda} (\tilde{x} - C\tilde{t}) + b(\check{x}) \quad (1)$$

where $b(\check{x}) = b_0 + K\check{x}$.

The governing equation of motion, continuity, thermal energy and nanoparticle fraction for peristaltic nanofluid can be written as [16]

$$\frac{\partial \tilde{u}}{\partial \tilde{x}} + \frac{\partial \tilde{v}}{\partial \tilde{y}} = 0, \quad (2)$$

$$\rho_f \left(\frac{\partial \tilde{u}}{\partial t} + \tilde{u} \frac{\partial \tilde{u}}{\partial x} + \tilde{v} \frac{\partial \tilde{u}}{\partial y} \right) = -\frac{\partial \tilde{p}}{\partial x} + \frac{\partial}{\partial x} S_{xx} + \frac{\partial}{\partial y} S_{xy} - \sigma B_0 \tilde{u} - \frac{\mu}{k} \tilde{u} + g \left[\frac{(1-F)\rho_{f_0}\zeta(T-T_0)}{(\rho_p - \rho_{f_0})(F-F_0)} \right] \quad (3)$$

$$\rho_f \left(\frac{\partial \tilde{v}}{\partial t} + \tilde{v} \frac{\partial \tilde{v}}{\partial x} + \tilde{u} \frac{\partial \tilde{v}}{\partial y} \right) = -\frac{\partial \tilde{p}}{\partial y} + \frac{\partial}{\partial x} S_{yx} + \frac{\partial}{\partial y} S_{yy} - \sigma B_0 \tilde{v} - \frac{\mu}{k} \tilde{v} + g \left[\frac{(1-F)\rho_{f_0}\zeta(T-T_0)}{(\rho_p - \rho_{f_0})(F-F_0)} \right] \quad (4)$$

$$(\rho c)_f \left(\frac{\partial T}{\partial t} + \tilde{u} \frac{\partial T}{\partial x} + \tilde{v} \frac{\partial T}{\partial y} \right) = \kappa \left(\frac{\partial^2 T}{\partial x^2} + \frac{\partial^2 T}{\partial y^2} \right) + (\rho c)_p D_B \left(\frac{\partial T}{\partial x} \frac{\partial F}{\partial x} + \frac{\partial F}{\partial y} \frac{\partial T}{\partial y} \right) + \frac{D_T}{T_0} \left(\left(\frac{\partial T}{\partial x} \right)^2 + \left(\frac{\partial T}{\partial y} \right)^2 \right) - \frac{\partial q_r}{\partial y} + Q_0, \quad (5)$$

$$\left(\frac{\partial F}{\partial t} + \tilde{u} \frac{\partial F}{\partial x} + \tilde{v} \frac{\partial F}{\partial y} \right) = D_B \left(\frac{\partial^2 F}{\partial x^2} + \frac{\partial^2 F}{\partial y^2} \right) + \frac{D_T}{T_0} \left(\frac{\partial^2 T}{\partial x^2} + \frac{\partial^2 T}{\partial y^2} \right) - k_1 (F - F_0), \quad (6)$$

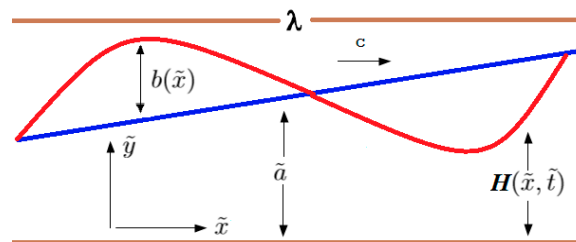


Figure 1. The geometry of the problem.

Now let us consider the assumptions of a long wavelength number and low Reynolds approximations in the sense of creeping flow. By using the dimensionless quantities in Equations (2)–(6), we get the resulting equations in a simplified form as

$$\frac{\partial^2 u}{\partial y^2} + We \frac{\partial}{\partial y} \left(\frac{\partial u}{\partial y} \right)^2 - \frac{1}{k} u - M^2 u - Gr_F \Phi + Gr_T \theta - \frac{\partial p}{\partial x} = 0, \quad (7)$$

$$\left(\frac{1 + R_n}{Pr} \right) \frac{\partial^2 \theta}{\partial y^2} + N_t \left(\frac{\partial \theta}{\partial y} \right)^2 + \beta + N_b \frac{\partial \theta}{\partial y} \frac{\partial \Phi}{\partial y} = 0, \quad (8)$$

$$\frac{\partial^2 \Phi}{\partial y^2} - \gamma \Phi + \frac{N_t}{N_b} \left(\frac{\partial^2 \theta}{\partial y^2} \right) = 0. \quad (9)$$

subject to the respective boundary conditions:

$$\Phi(0) = 0, \quad \frac{\partial u(0)}{\partial y} = 0, \quad \theta(0) = 0, \quad (10)$$

$$\Phi(h) = 1, \quad \theta(h) = 1, \quad u(h) = 0 \quad (11)$$

In the presence of a magnetic field, the entropy generation can be derived from energy and entropy balance for the case of heat and mass transfer as [43]

$$S_{gen} = \frac{\mathcal{K}_{nf}}{T_0^2} (\nabla T)^2 + \frac{\mu_{nf}}{k T_0} \left[2 \left(\frac{\partial \tilde{u}}{\partial x} \right)^2 + 2 \left(\frac{\partial \tilde{v}}{\partial y} \right)^2 + \left(\frac{\partial \tilde{u}}{\partial y} + \frac{\partial \tilde{v}}{\partial x} \right)^2 \right] + \frac{\sigma B_0^2}{T_0} \left(\frac{\partial \tilde{u}}{\partial y} \right)^2 + \frac{R D_B}{F_0} (\nabla F)^2 + \frac{R D_B}{T_0} (\nabla F \cdot \nabla T) \quad (12)$$

The dimensionless form of the entropy generation number can be expressed as follows:

$$N_s = \frac{S_{gen}}{S_g} = \left(\frac{\mathcal{K}_{nf}}{\mathcal{K}_f} \right) \left(\left(\frac{\partial \theta}{\partial y} \right)^2 \right) + (1 + M^2) Br \frac{1}{\Omega} \left(\frac{\mu_{nf}}{\mu_f} \right) \left(\frac{\partial u}{\partial y} \right)^2 + \Gamma \left(\frac{\Lambda}{\Omega} \right)^2 \left(\frac{\partial \Phi}{\partial y} \right)^2 + \zeta \left(\frac{\partial \theta}{\partial y} \right) \left(\frac{\partial \Phi}{\partial y} \right), \quad (13)$$

where $\Omega, B_r, \Lambda, \Gamma, \zeta$ are the dimensionless temperature difference, Brinkman number, concentration difference, diffusive coefficient and constant parameter, represented as

$$\Omega = \frac{(T_1 - T_0)}{T_0}, B_r = \frac{\bar{c}^2 \mu_f}{k \mathcal{K}_f (T_1 - T_0)}, \zeta = \frac{RD_B T_0}{\mathcal{K}_f} \left(\frac{F_1 - F_0}{T_1 - T_0} \right), \Gamma = \frac{RD_B F_0}{\mathcal{K}_f}, \Lambda = \frac{F_1 - F_0}{F_0}. \tag{14}$$

For nanofluid, the viscosity model and thermal conductivity can be defined as [50]

$$\mu_{nf} = \frac{\mu_f}{(1 - \Phi)^{2.5}}, \mathcal{K}_{nf} = \frac{\kappa_p + 2\kappa_f + 2\bar{\Phi}(\kappa_p - \kappa_f)}{\kappa_p + 2\kappa_f - \bar{\Phi}(\kappa_p - \kappa_f)} \kappa_f \tag{15}$$

where μ_f, κ_f and κ_p , are the viscosity of base fluid, thermal conductivities of the nanofluid and nanoparticle, respectively.

3. Solution of Problem

With the help of HPM [16], Equations (7)–(9) can be written as:

$$\mathcal{H}(w, \bar{q}) = (1 - \hat{q})(L_1(w) - L_1(\bar{w}_0)) + \hat{q} \left(L_1(w) + We \frac{\partial}{\partial y} \left(\frac{\partial w}{\partial y} \right)^2 + Gr_T \Theta - Gr_F \vartheta - \frac{\partial p}{\partial x} \right), \tag{16}$$

$$\mathcal{H}(\Theta, \bar{q}) = (1 - \hat{q})(L_2(\Theta) - L_2(\bar{\Theta}_0)) + \hat{q} \left(L_2(\Theta) + \frac{Pr}{1 + RePr} \left(N_b \frac{\partial \vartheta}{\partial y} \frac{\partial \Theta}{\partial y} + N_t \left(\frac{\partial \vartheta}{\partial y} \right)^2 \right) + \frac{Pr\beta}{1 + RePr} \right) \tag{17}$$

$$\mathcal{H}(\vartheta, \bar{q}) = (1 - \hat{q})(L_2(\vartheta) - L_2(\bar{\vartheta}_0)) + \hat{q} \left(L_2(\vartheta) + \frac{N_t}{N_b} \left(\frac{\partial^2 \Theta}{\partial y^2} \right) - \gamma \vartheta \right), \tag{18}$$

and the initial guess and linear operators for Equations (16)–(18) are defined as

$$\bar{w}_0 = \frac{\cosh N^2 y - \cosh N^2 h}{\cosh N^2 h}, \tag{19}$$

$$\bar{\vartheta}_0 = \bar{\Theta}_0 = \frac{y}{h}. \tag{20}$$

$$L_1 = \frac{\partial^2}{\partial y^2} - M^2 - \frac{1}{k} \tag{21}$$

$$L_2 = \frac{\partial^2}{\partial y^2}, \tag{22}$$

which defines the following expansion:

$$\vartheta(x, y) = \vartheta_0(x, y) + \hat{q} \vartheta_1(x, y) + \hat{q}^2 \vartheta_2(x, y) + \dots, \tag{23}$$

$$\Theta(x, y) = \Psi_0(x, y) + \hat{q} \Psi_1(x, y) + \hat{q}^2 \Psi_2(x, y) + \dots, \tag{24}$$

$$w(x, y) = w_0(x, y) + \hat{q} w_1(x, y) + \hat{q}^2 w_2(x, y) + \dots, \tag{25}$$

Using the expansion series defined in the terms mentioned in Equations (23)–(25) and incorporating them into the Equations (16)–(18) we get a system of linear differential equations and their relevant boundary conditions. Applying the scheme of HPM and comparing the powers of \hat{q} , we obtain the solution as $\hat{q} \rightarrow 1$. We obtained the temperature distribution, velocity profile, and concentration profile.

Utilizing the expanding arrangement characterized in terms of $(\vartheta(x, y), \Theta(x, y))$ and $(w(x, y))$ as referenced in Equations (23)–(25) and using into the Equations (16)–(18), we get an arrangement of direct differential equations with their significant limit conditions. By contrasting the forces of

$\hat{q} \rightarrow 1$, we apply the scheme of HPM to determine the arrangement as $q' \rightarrow 1$, and obtain the required arrangements of temperature circulation, speed profile, and fixation profile.

4. Results and Discussion

In this section the obtained results are discussed. As shown in Figure 2, for higher values of N_b and N_t the temperature profile increases. This is because the Brownian motion creates micro-mixing, which increases thermal conductivity. Figure 3 shows that concentration force has the opposite behavior for various values of N_b and N_t . It is observed from Figure 4 that pressure distribution has opposite effect for the various values of thermal Grashof parameter Gr_T . and basic density Grashof number Gr_F . The thermal Grashof parameter proclaims the general impact of thick hydrodynamic power and thermal buoyancy forces. For $Gr_T < 1$, the peristaltic routine is ruled by viscous powers, which is the other way around for $Gr_T > 1$. The Gr_F parameter is basically the proportion of species buoyancy forces to the thick hydrodynamic forces. For a situation where the two forces are equivalent (e.g., $Gr_F = 1$), velocity will be minimized. We can conclude from Figure 5a that pressure rise reduces for the larger values of magnetic parameter M , which shows the fact that pressure can be controlled by using the suitable magnetic field. Also, it is concluded from this figure that flow can pass easily without imposing higher pressure inside the channel. From Figures 5b and 6, it is observed that friction force has completely the opposite behavior for the different values of the same physical parameters as compared with pressure rise distribution. Figure 7 shows a comparison of the graphical results of pressure rise and velocity profile. In Equation (7), by taking $W_e = 0, M = 0, \kappa \rightarrow \infty, Gr_F = 0, Gr_T = 0$, the current results can be reduced to the results obtained by Shapiro et al. [39] for the Newtonian case. Further results can also be reduced to the similar results obtained by Gupta and Seshadri [41] and Mekheimer [42] by taking $W_e = 0, \kappa \rightarrow \infty, Gr_F = 0, Gr_T = 0$.

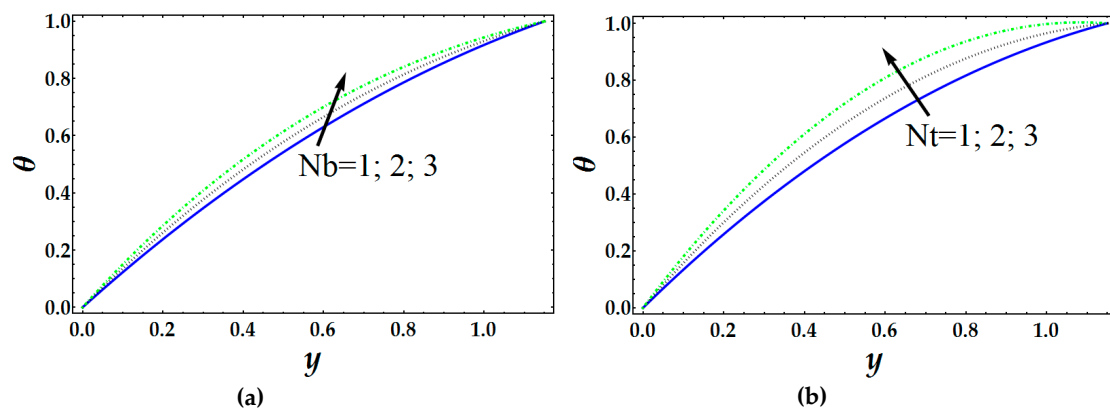


Figure 2. Temperature profile for various values of N_b and N_t .

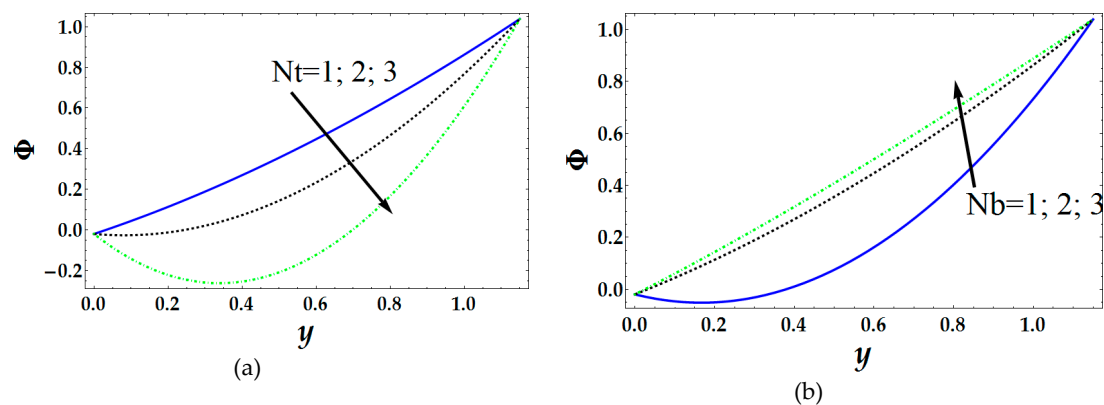


Figure 3. Concentration profile for various values of N_t and N_b .

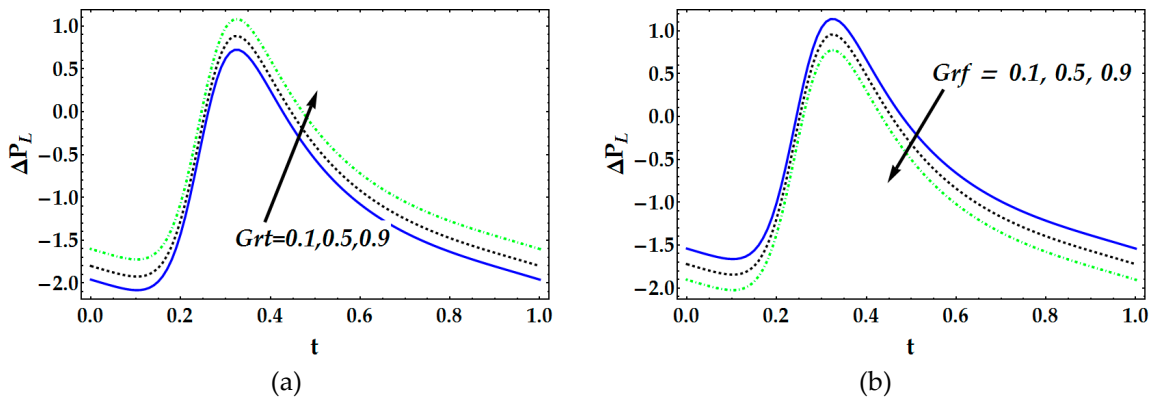


Figure 4. Pressure rise distribution for various values of Gr_t and Gr_f .

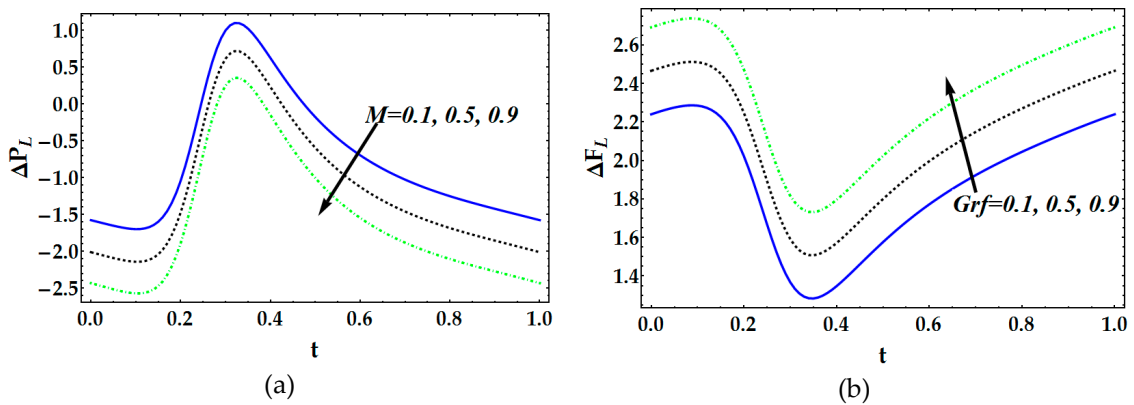


Figure 5. Pressure distribution for various values of M and friction force profile for various values of Gr_f .

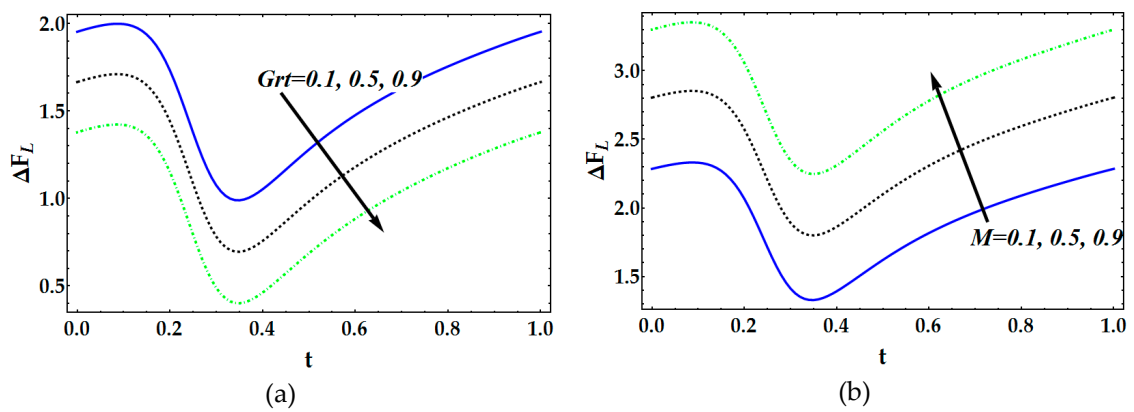


Figure 6. Friction force for various values of Gr_t and M .

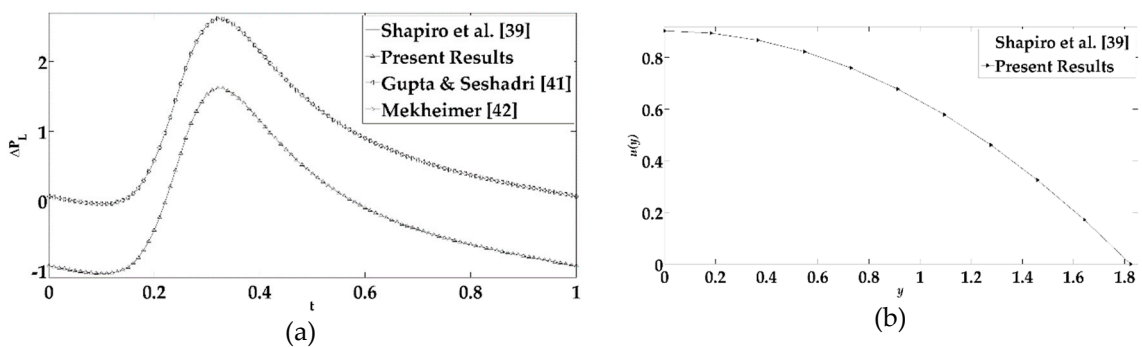


Figure 7. (a) Comparison of pressure rise; (b) comparison of velocity profile.

From Table 1, the R-square entropy generation for various values of magnetic parameter M is determined to be 0.809, meaning that approximately 81% of the variability of entropy generation is explained by parameter M in the model. On the other hand, the adjusted R-square 0.799 indicates that about 80% of the variability of entropy generation is accounted for Magnetic parameter M by the model. The entropy generation value for Brownian motion parameter N_b is 0.998, which indicates that approximately 99% of the variability of entropy is due to parameter N_b in the model, while the adjusted R-square 0.999 indicates that about 99% of the variability of entropy is accounted for N_b by the model. In the R-square, the value of entropy generation for thermophoresis parameter N_t is 0.403, which reveals that approximately 40% of the variability of entropy is explained by parameter N_t in the model, while the adjusted R-square 0.370 indicates that about 37% of the variability of entropy is accounted for N_t by the model. The entropy value for different values of B_r is 1.00 with 100% of the variability of entropy accounted for parameter B_r in the model, while the adjusted R-square 1.00 indicates that about 100% of the variability of entropy is accounted for B_r by the Model.

Table 1. Model summary.

Model	R	R Square	Adjusted R Square	Standard Error of the Estimate
1	0.900 ^a	0.809	0.799	0.7558884
2	0.999 ^a	0.998	0.998	0.0550427
3	0.635 ^a	0.403	0.370	4.6675041
4	1.000 ^a	1.000	1.000	0.19437519

^a Predictors: (Constant), M.

From Table 2, a decrease of -2.562 in entropy for independent variable M and an increase of 2.029 in Entropy for N_b can be concluded. Similarly, an increase of 6.307 in entropy for parameter N_t and an increase of 68.492 in entropy for B_r scores can be concluded for every single-unit increase in Iv , assuming all other variables in the model are constant. Table 3 is plotted to break down the relationship of entropy generation for some delicate parameters. It is determined from these outcomes that a huge impeccable significant positive connection exists between Brinkman number B_r and its entropy generation at 0.01 level. A solid positive relationship has been seen from the connection results between entropy and the parameters N_t and N_b . An extremely negative relationship was seen between M and its entropy.

Table 2. Coefficients.

Model		Unstandardized Coefficients		Standardized Coefficients	T	Significant
		B	Standard Error	Beta		
1	(Constant)	74.223	0.351		211.381	0.000
	M	-2.562	0.293	-0.900	-8.739	0.000
2	(Constant)	29.097	0.026		1137.975	0.000
	M	2.049	0.021	0.999	95.977	0.000
3	(Constant)	65.565	2.168		30.239	0.000
	M	6.307	1.810	0.635	3.485	0.003
4	(Constant)	1.359	0.090		15.056	0.000
	M	68.492	0.075	1.000	908.676	0.000

Table 3. Correlation table between entropy generation and parameters. **.

Entropy and Parameters	N_s V_s B_r	N_s V_s N_t	N_s V_s N_b	N_s V_s M
Values range	0.1 to 2.0	0.1 to 2.0	0.1 to 2.0	0.1 to 2.0
N	20	20	20	20
Pearson Correlation	1.000 **	0.635 **	0.999 **	0.900 **
Siganificant (2-tailed)	0.000	0.003	0.000	0.000
Remarks	Perfect Relation	Strong Positive Relation	Strong Positive Relation	Very Strong Negative Relations

** Correlation is significant at the 0.01 level (2-tailed).

5. Conclusions

The following outcomes demonstrated through this study are:

- Temperature profile increases with higher values of N_b and N_t .
- Pressure distribution and friction have an inverse conduct for bigger estimations of the magnetic parameter, Brownian movement parameter and thermophoresis parameter.
- The variability of entropy generation is 81% for the values of M , while 99% variability for the parameter N_b .
- The variability of entropy generation is 40% for the values of N_t , while 100% variability for the parameter B_r .

Author Contributions: M.A.A. conceived, mathematical formulation and applied the method. M.I. did literature survey, data collection and analysis.

Conflicts of Interest: The authors declare no conflicts of interest.

Nomenclature

\tilde{u}, \tilde{v}	velocity components (m/s)
\tilde{x}, \tilde{y}	Cartesian coordinate (m)
\tilde{p}	pressure in fixed frame (N/m ²)
\tilde{a}	wave amplitude (m)
$b(\tilde{x})$	width of the channel (m)
\tilde{c}	wave velocity (m/s)
Pr	Prandtl number
Re	Reynolds number
Rn	Radiation parameter
\tilde{t}	time (s)
Gr_F	basic density Grashof number
Gr_T	thermal Grashof number
N_b	Brownian motion parameter
N_t	thermophoresis parameter
$\bar{K}(\ll 1)$	constant
B_0	magnetic field (T)
We	Weissenberg number
Q	volume flow rate (m ³ /s)
T, F	temperature (K) and concentration
g	acceleration due to gravity (m/s ²)
D_B	Brownian diffusion coefficient (m ² /s)
D_T	thermophoretic diffusion coefficient (m ² /s)
K	mean absorption constant
M	Hartman number
\mathbf{S}	stress tensor
\tilde{k}	porosity parameter

Greek Symbols

κ	nanofluid thermal conductivity (W/m K)
μ	viscosity of the fluid (N s/m ²)
Φ	nanoparticle volume fraction
σ	electrical conductivity (S/m)
δ	wave number (m ⁻¹)
c_p	effective heat capacity of nanoparticle (J/K)
ν	nanofluid kinematic viscosity (m ² /s)
$(\rho)_p$	nanoparticle mass density (kg/m ³)
ρ_f	fluid density (kg/m ³)
ρ_{f_0}	fluid density at the reference temperature (T_0) (kg/m ³)
ζ	volumetric expansion coefficient of the fluid
$(\rho c)_f$	heat capacity of fluid (J/K)
λ	wavelength (m)
Φ	amplitude ratio
μ_{nf}	viscosity of nanofluid
θ	Temperature

References

- Villone, M.M.; Greco, F.; Hulsen, M.A.; Maffettone, P.L. Simulation of an elastic particle in Newtonian and Viscoelastic fluids subjected to confined shear flow. *J. Non-Newton. Fluid Mech.* **2014**, *210*, 47–55. [[CrossRef](#)]
- Hatami, M.; Domairry, G. Transient vertically motion of a soluble particle in a Newtonian fluid media. *J. Powder Technol.* **2014**, *253*, 481–485. [[CrossRef](#)]
- Liu, J.; Zhu, C.; Fu, T.; Ma, Y.; Li, H. Numerical simulation of the interaction between three equal interval parallel bubbles rising in non-Newtonian fluid. *Chem. Eng. Sci.* **2013**, *93*, 55–66. [[CrossRef](#)]
- Hatami, M.; Ganji, D.D. Natural convection of sodium alginate Non-Newtonian nanofluid flow between two vertical flat plates by analytical and numerical methods. *Case Stud. Therm. Eng.* **2014**, *2*, 14–22. [[CrossRef](#)]
- Chamkha, A.J. On laminar hydromagnetic mixed convection flow in a vertical channel with symmetric and asymmetric wall heating conditions. *Int. J. Heat Mass Transf.* **2002**, *45*, 2509–2525. [[CrossRef](#)]
- Umavathi, J.C.; Kumar, J.P.; Chamkha, A.J.; Pop, I. Mixed convection in a vertical porous channel. *Transp. Porous Media* **2005**, *61*, 315–335. [[CrossRef](#)]
- Chamkha, A.J. Unsteady laminar hydromagnetic fluid–particle flow and heat transfer in channels and circular pipes. *Int. J. Heat Fluid Flow* **2000**, *21*, 740–746. [[CrossRef](#)]
- Ghalambaz, M.; Behseresht, A.; Behseresht, J.; Chamkha, A. Effects of nanoparticles diameter and concentration on natural convection of the Al₂O₃–water nanofluids considering variable thermal conductivity around a vertical cone in porous media. *Adv. Powder Technol.* **2015**, *26*, 224–235. [[CrossRef](#)]
- Reddy, P.S.; Chamkha, A.J. Soret and Dufour effects on MHD convective flow of Al₂O₃–water and TiO₂–water nanofluids past a stretching sheet in porous media with heat generation/absorption. *Adv. Powder Technol.* **2016**, *27*, 1207–1218. [[CrossRef](#)]
- Chamkha, A. Fully developed free convection of a micropolar fluid in a vertical channel. *Int. Commun. Heat Mass Transf.* **2002**, *29*, 1119–1127. [[CrossRef](#)]
- Kumar, J.P.; Umavathi, J.C.; Chamkha, A.J.; Pop, I. Fully-developed free-convective flow of micropolar and viscous fluids in a vertical channel. *Appl. Math. Model.* **2010**, *34*, 1175–1186. [[CrossRef](#)]
- Chamkha, A.J.; Grosan, T.; Pop, I. Fully developed mixed convection of a micropolar fluid in a vertical channel. *Int. J. Fluid Mech. Res.* **2003**, *30*, 251–263. [[CrossRef](#)]
- Choi, S.U.S.; Eastman, J.A. Enhancing thermal conductivity of fluids with nanoparticles. *Mater. Sci.* **1995**, *231*, 99–105.
- Eastman, J.A.; Choi, U.S.; Li, S.; Soyez, G.; Thompson, L.J.; DiMelfi, R.J. Novel thermal properties of nanostructured materials. *Mater. Sci. Forum* **1999**, *312*, 629–634. [[CrossRef](#)]
- Latham, T.W. Fluid Motions in a Peristaltic Pump. Ph.D. Thesis, Massachusetts Institute of Technology, Cambridge, MA, USA, 1966.

16. Abbas, M.A.; Bai, Y.Q.; Rashidi, M.M.; Bhatti, M.M. Application of drug delivery in magnetohydrodynamics peristaltic blood flow of nanofluid in a non-uniform channel. *J. Mech. Med. Biol.* **2016**, *16*, 1650052. [[CrossRef](#)]
17. Bhatti, M.M.; Abbas, M.A.; Rashidi, M.M. Combine effects of magnetohydrodynamics (MHD) and partial slip on peristaltic blood flow of Ree–Eyring fluid with wall properties. *Eng. Sci. Technol. Int. J.* **2016**, *19*, 1497–1502. [[CrossRef](#)]
18. Salleh, S.; Bachok, N.; Arifin, N.; Ali, F.; Pop, I. Magnetohydrodynamics flow past a moving vertical thin needle in a nanofluid with stability analysis. *Energies* **2018**, *11*, 3297. [[CrossRef](#)]
19. Cong, R.; Ozaki, Y.; Machado, B.; Das, P. Constructal Design of a Rectangular Fin in a Mixed Convective Confined Environment. *Inventions* **2018**, *3*, 27. [[CrossRef](#)]
20. Sadiq, M.; Alsabery, A.; Hashim, I. MHD Mixed Convection in a Lid-Driven Cavity with a Bottom Trapezoidal Body: Two-Phase Nanofluid Model. *Energies* **2018**, *11*, 2943. [[CrossRef](#)]
21. Das, P.K.; Mahmud, S.; Humaira Tasnim, S.; Sadrul Islam AK, M. Effect of surface waviness and aspect ratio on heat transfer inside a wavy enclosure. *Int. J. Numer. Methods Heat Fluid Flow* **2003**, *13*, 1097–1122. [[CrossRef](#)]
22. Abbas, M.A.; Faraz, N.; Bai, Y.Q.; Khan, Y. Analytical study of the non-orthogonal stagnation point flow of a micro polar fluid. *J. King Saud Univ. Sci.* **2017**, *29*, 126–132. [[CrossRef](#)]
23. Umavathi, J.C.; Chamkha, A.J.; Sridhar KS, R. Generalized plain Couette flow and heat transfer in a composite channel. *Transp. Porous Media* **2010**, *85*, 157–169. [[CrossRef](#)]
24. Bhatti, M.M.; Abbas, M.A. Simultaneous effects of slip and MHD on peristaltic blood flow of Jeffrey fluid model through a porous medium. *Alex. Eng. J.* **2016**, *55*, 1017–1023. [[CrossRef](#)]
25. Abbas, M.A.; Bai, Y.Q.; Bhatti, M.M.; Rashidi, M.M. Three-dimensional peristaltic flow of hyperbolic tangent fluid in non-uniform channel having flexible walls. *Alex. Eng. J.* **2016**, *55*, 653–662. [[CrossRef](#)]
26. Chamkha, A.J.; Al-Subaie, M.A. Hydromagnetic buoyancy-induced flow of a particulate suspension through a vertical pipe with heat generation or absorption effects. *Turk. J. Eng. Environ. Sci.* **2010**, *33*, 127–134.
27. Takhar, H.S.; Chamkha, A.J.; Nath, G. Unsteady flow and heat transfer on a semi-infinite flat plate with an aligned magnetic field. *Int. J. Eng. Sci.* **1999**, *37*, 1723–1736. [[CrossRef](#)]
28. Chamkha, A.J.; Khaled, A.R.A. Hydromagnetic combined heat and mass transfer by natural convection from a permeable surface embedded in a fluid-saturated porous medium. *Int. J. Numer. Methods Heat Fluid Flow* **2000**, *10*, 455–477. [[CrossRef](#)]
29. Chamkha, A.J. Flow of two-immiscible fluids in porous and nonporous channels. *J. Fluids Eng.* **2000**, *122*, 117–124. [[CrossRef](#)]
30. Chamkha, A. Unsteady flow of a dusty conducting fluid through a pipe. *Mech. Res. Commun.* **1994**, *21*, 281–288. [[CrossRef](#)]
31. Chamkha, A.J. Non-Darcy fully developed mixed convection in a porous medium channel with heat generation/absorption and hydromagnetic effects. *Numer. Heat Transf. Part A Appl.* **1997**, *32*, 653–675. [[CrossRef](#)]
32. Umavathi, J.C.; Chamkha, A.J.; Mateen, A.; Al-Mudhaf, A. Unsteady oscillatory flow and heat transfer in a horizontal composite porous medium channel. *Nonlinear Anal. Model. Control* **2009**, *14*, 397–415.
33. Umavathi, J.C.; Chamkha, A.J.; Mateen, A.; Al-Mudhaf, A. Unsteady two-fluid flow and heat transfer in a horizontal channel. *Heat Mass Transf.* **2005**, *42*, 81. [[CrossRef](#)]
34. Chamkha, A.J. Unsteady laminar hydromagnetic flow and heat transfer in porous channels with temperature-dependent properties. *Int. J. Numer. Methods Heat Fluid Flow* **2001**, *11*, 430–448. [[CrossRef](#)]
35. Chamkha, A.J. Hydromagnetic two-phase flow in a channel. *Int. J. Eng. Sci.* **1995**, *33*, 437–446. [[CrossRef](#)]
36. Ismael, M.A.; Pop, I.; Chamkha, A.J. Mixed convection in a lid-driven square cavity with partial slip. *Int. J. Therm. Sci.* **2014**, *82*, 47–61. [[CrossRef](#)]
37. Parvin, S.; Nasrin, R.; Alim, M.A.; Hossain, N.F.; Chamkha, A.J. Thermal conductivity variation on natural convection flow of water–alumina nanofluid in an annulus. *Int. J. Heat Mass Transf.* **2012**, *55*, 5268–5274. [[CrossRef](#)]
38. Ghalambaz, M.; Doostani, A.; Izadpanahi, E.; Chamkha, A.J. Phase-change heat transfer in a cavity heated from below: The effect of utilizing single or hybrid nanoparticles as additives. *J. Taiwan Inst. Chem. Eng.* **2017**, *72*, 104–115. [[CrossRef](#)]
39. Shapiro, A.H.; Jaffrin, M.Y.; Weinberg, S.L. Peristaltic pumping with long wavelengths at low Reynolds number. *J. Fluid Mech.* **1969**, *37*, 799–825. [[CrossRef](#)]

40. Zaraki, A.; Ghalambaz, M.; Chamkha, A.J.; Ghalambaz, M.; De Rossi, D. Theoretical analysis of natural convection boundary layer heat and mass transfer of nanofluids: Effects of size, shape and type of nanoparticles, type of base fluid and working temperature. *Adv. Powder Technol.* **2015**, *26*, 935–946. [[CrossRef](#)]
41. Gupta, B.B.; Seshadri, V. Peristaltic pumping in non-uniform tubes. *J. Biomech.* **1976**, *9*, 105–109. [[CrossRef](#)]
42. Mekheimer, K.S. Peristaltic flow of blood under effect of a magnetic field in a non-uniform channel. *Appl. Math. Comput.* **2004**, *153*, 763–777. [[CrossRef](#)]
43. Rashidi, M.M.; Bhatti, M.M.; Abbas, M.A.; Ali ME, S. Entropy Generation on MHD Blood Flow of Nanofluid Due to Peristaltic Waves. *Entropy* **2016**, *18*, 117. [[CrossRef](#)]
44. Torabi, M.; Zhang, K.; Karimi, N.; Peterson, G.P. Entropy generation in thermal systems with solid structures—A concise review. *Int. J. Heat Mass Transf.* **2016**, *97*, 917–931. [[CrossRef](#)]
45. Biswal, P.; Basak, T. Entropy generation vs energy efficiency for natural convection based energy flow in enclosures and various applications: A review. *Renew. Sustain. Energy Rev.* **2017**, *80*, 1412–1457. [[CrossRef](#)]
46. Rashidi, M.M.; Abbas, M.A. Effect of Slip Conditions and Entropy Generation Analysis with an Effective Prandtl Number Model on a Nanofluid Flow through a Stretching Sheet. *Entropy* **2017**, *18*, 414. [[CrossRef](#)]
47. Qing, J.; Bhatti, M.M.; Abbas, M.A.; Rashidi, M.M.; Ali, M.E.S. Entropy Generation on MHD Casson Nanofluid Flow over a Porous Stretching/Shrinking Surface. *Entropy* **2016**, *18*, 123. [[CrossRef](#)]
48. Bhatti, M.M.; Abbas, T.; Rashidi, M.M. Numerical study of entropy generation with nonlinear thermal radiation on magnetohydrodynamics non-newtonian nanofluid through a porous shrinking sheet. *J. Magn.* **2016**, *21*, 468–475. [[CrossRef](#)]
49. Abbas, M.A.; Bai, Y.; Rashidi, M.M.; Bhatti, M.M. Analysis of Entropy Generation in the Flow of Peristaltic Nanofluids in Channels with Compliant Walls. *Entropy* **2016**, *18*, 90. [[CrossRef](#)]
50. Mahian, O.; Kianifar, A.; Kleinstreuer, C.; Moh'd, A.A.N.; Pop, I.; Sahin, A.Z.; Wongwises, S. A review of entropy generation in Nanofluid flow. *Int. J. Heat Mass Transf.* **2013**, *65*, 514–532. [[CrossRef](#)]



© 2019 by the authors. Licensee MDPI, Basel, Switzerland. This article is an open access article distributed under the terms and conditions of the Creative Commons Attribution (CC BY) license (<http://creativecommons.org/licenses/by/4.0/>).